

Comparison of the kinetic performance and retentivity of sub-2  $\mu\text{m}$  core-shell, hybrid and conventional bare silica phases in hydrophilic interaction chromatography.

James C. Heaton, David V. McCalley\*

Centre for Research in Biosciences, University of the West of England, Frenchay, Bristol

BS16 1QY, UK

\*Corresponding author: [david.mccalley@uwe.ac.uk](mailto:david.mccalley@uwe.ac.uk)

[Keywords: HILIC; core-shell; Column efficiency; Diffusion; Buffers](#)

## Abstract

The separation performance and retention properties of four sub-2  $\mu\text{m}$  underivatized silica materials were evaluated in the hydrophilic interaction chromatography (HILIC) mode. These included an organic/inorganic hybrid silica, conventional silica, narrow particle size distribution silica and a core-shell silica. Van Deemter characterisation was performed using conditions to give high retention factors ( $k= 5.5-6.0$ ) with 10 cm columns to limit the contribution of extra-column dispersion. The core-shell 1.6  $\mu\text{m}$  bare silica (Cortecs) was shown to be kinetically superior to fully porous particle types. Little column-to-column variation in the reduced  $b$ -coefficient was observed for the test analytes as corroborated by arrested elution experiments. However, the reduced  $b$ -coefficient was shown to be different between analytes e.g. cytosine versus nortriptyline. It is speculated that the nature of the retention mechanism (hydrophilic versus ionic retention) and solute physiochemical properties perhaps influence the  $b$ -coefficient. Maxwell-Effective Medium Theory (EMT) applied to results for a wider range of solutes indicated that the intra-particle diffusion ( $D_{part}$ ) behaviour for individual compounds is broadly similar irrespective of the particle morphology in HILIC. Finally, the impact of varying buffer concentration for a test mix showed that retention and peak shape varied considerably between different silicas. High efficiency separations can be achieved for hydrophilic and basic solutes using a combination of sub-2  $\mu\text{m}$  core shell bare silica particles and appropriate buffer concentrations.

## 1. Introduction

Hydrophilic interaction liquid chromatography (HILIC) is becoming increasingly popular for the separation of polar or ionised solutes. In HILIC, retention is thought to occur principally by partitioning between the hydro-organic mobile phase (> 70% ACN v/v) and a water-rich layer which is held at the stationary phase surface [1]. Additionally, adsorption and ionic processes contribute to the retention mechanism, due to specific interactions between solute and stationary phase. Many stationary phase types are now available for HILIC. Bare silica is popular, and can be a useful alternative to reversed-phase (RP) for the separation of basic pharmaceuticals [2]. One of the major drawbacks of RP is the overload of ionised basic compounds resulting in poor peak shape [3]. Using bare silica in HILIC, symmetrical peak shapes can be obtained for some charged bases with higher sample loads [2] regardless of the particle morphology [4]. Furthermore, the high concentrations of organic solvents used in HILIC mobile phases make the technique very suitable for use with detection techniques such as electrospray ionisation-mass spectrometry and charged aerosol detection (CAD).

Modern sub-3  $\mu\text{m}$  superficially porous particles with relatively thick shells have been shown as a useful adaptation of earlier pellicular materials [5,6], which suffered from low sample capacity due to their thin shells. These new materials can generate almost the same efficiency as fully porous sub-2  $\mu\text{m}$  particles but at lower pressure drops [7]. The lowest reduced plate heights have been obtained from wider-bore 4.6 mm columns rather than the more convenient 2.1 mm ID format [8]. However, the superior kinetic performance of shell compared with totally porous particles of the same diameter has still not been fully explained [9,10]. Shell particles can be manufactured with a very narrow particle size distribution [11]. While this factor *per se* may not be the reason for the substantially lower eddy dispersion observed for shell particles, it is possible that it improves the packing properties of these materials [9]. The roughness of some types of shell particle may also improve the packed bed stability and homogeneity [12]. Also, the superior thermal conductivity of shell particles assists in radial heat dissipation. Otherwise, frictional heating can adversely affect the performance at high flow [10]. This factor explains why even 4.6 mm columns of shell particles can be used under some conditions. Furthermore, axial dispersion has been shown to be reduced in reversed-phase shell columns due to restricted diffusion from the presence of a solid-core [13–15]. Another development in particle synthesis has been that of fully porous hybrid organo-silica phases, giving rise to pH stable ( $w^w\text{pH}$  2-10, possibly  $w^w\text{pH}$  1-12 for short periods), sub-2  $\mu\text{m}$  particles for ultra-high pressure chromatography (600-1000 bar) [16]. In contrast, a practical limitation of conventional silica-based shell materials (which are not currently available based on this hybrid

technology), is their reduced stability at higher pH (> 7, or > 8 for short periods) making them less flexible for method development. This is even more important in HILIC, since the hydrolytic stability offered by chemical modification is absent for bare silica phases.

The aim of this study was to compare the kinetic and retention characteristics of different sub-2  $\mu\text{m}$  bare silica columns in 2.1 mm formats (HSS, TITAN, Cortecs, BEH) in the HILIC mode. These represent a wide range of recently available materials comprising conventional, narrow particle size distribution, core-shell and inorganic/organic hybrid silica particles. Bare silica is less suitable for the analysis of strongly acidic compounds due to electrostatic repulsion from ionised silanol groups, thus our study has concentrated instead on neutral and basic solutes [17]. Kinetic performance was assessed by evaluating the plate count versus flow of each phase and supporting the observations with data from arrested elution experiments. Arrested elution experiments also allowed for further characterisation of the intrinsic column performance with respect to the reduced  $b$ -coefficient. Results were also examined using kinetic plot representation of data which employs non-reduced van Deemter coefficients which are of relevance to the practitioner. In order to highlight differences in the retentivity of each of the investigated phases, variation in buffer concentration at fixed organic concentration was also performed.

## 2. Experimental

### 2.1 Chemicals and reagents

HPLC grade acetonitrile (ACN) and tetrahydrofuran (THF) were purchased from Fisher Scientific (Loughborough, UK). Ammonium formate, formic acid, toluene, benzylamine, diphenhydramine, phenylephrine, uracil, 5-(hydroxymethyl)uridine, cytosine, nortriptyline, propranolol and procainamide were all obtained from Sigma-Aldrich (Poole, UK). A polystyrene calibration kit (MW 575-2,851,000) for inverse size exclusion chromatography (ISEC) was obtained from Varian Inc. / Agilent Technologies (Stockport, UK). Water at 18.2  $\text{m}\Omega$  was from a Purite Onedeo purifier (Thame, UK). Mobile phases were prepared as pre-mixed solutions as shown in Table 1. Note for nortriptyline, the buffer concentration was varied to allow maintenance of high  $k$  without using less than 5% water in the mobile phase, which is a common lower limit often employed in HILIC. The peak shape for nortriptyline was excellent on all columns under the conditions in Table 1 (see below).

### 2.2 Apparatus and methodology

Flow rate versus plate height experiments and Cox plot analysis ( $k$  versus  $1/[M^+]$ ) were performed on a Waters Acquity Classic Ultra Pressure Liquid Chromatograph (UPLC, Waters Corp., Milford, MA, USA). The instrument included a binary solvent manager, sample manager, diode array detector (DAD, 80 Hz data collection) equipped with a 500 nL flow cell and was operated using Empower 2 software. The  $V_{\text{ext}}$  of the UPLC system was approximately 12.0  $\mu\text{L}$  and the extra-column variance ( $\sigma^2$ ) of the UPLC at 0.4 mL/min was around 3.5  $\mu\text{L}^2$ , measured using similar mobile phases as in Table 1. Peak parking experiments were performed using a model 1290 Infinity ultra-high pressure liquid chromatograph (UHPLC, Agilent Technologies, Walbronn, Germany) operated using Chemstation software. This instrument included a binary pump, column compartment, autosampler and DAD (0.6  $\mu\text{L}$  flow cell). The  $V_{\text{ext}}$  of the Agilent system was 13.6  $\mu\text{L}$  and the extra-column variance ( $\sigma^2$ ) around 5.0  $\mu\text{L}^2$  at 0.4 mL/min. Arrested elution experiments were performed (0.4 mL/min flow) using a 6-port, 2-position dual column switching valve, which allowed the measurement column to be held under pressure while an identical dummy column of the same particle size and dimensions was used in place during switching times. The arrested elution times used were 0, 2, 5, 10, 20, 30 and 60 minutes. Column hold-up volumes ( $V_m$ ) were determined using toluene in the injected sample which was dissolved in the exact mobile phase in each case. Columns were maintained at 30 °C in the column compartment throughout all experiments. All efficiency and extra-column peak measurements were made at  $5\sigma$  (4.4% peak height). Corrections for extra-column effects at each flow rate were obtained using a zero-volume connector. However, due to the high  $k$  used for the construction of each van Deemter curve and the length of the columns used, these corrections were very small. Detector settings were 270 nm for cytosine and procainamide, 240 nm for nortriptyline and 210 nm for diphenhydramine, benzylamine and phenylephrine on both chromatographic systems. 1.0  $\mu\text{L}$  (full loop on Acquity UPLC) injections of 10 ppm solutions dissolved in the exact mobile phase were used in all experiments except for benzylamine and phenylephrine which were at 50 ppm. The bare silica columns (all 100 x 2.1 mm ID) used were BEH HILIC (1.7  $\mu\text{m}$  particle size, hybrid silica), Prototype HSS HILIC (1.8  $\mu\text{m}$  particle size, conventional silica), Cortecs HILIC (1.6  $\mu\text{m}$  particle size, shell particles with  $\rho = 0.7$ ) from Waters Corp. (Milford, USA) and Prototype TITAN HILIC (1.9  $\mu\text{m}$  particle, narrow particle size distribution) from Supelco (Bellefonte, PA, USA). The column external porosity was measured by ISEC using a series of polystyrene standards dissolved in and eluted with pure THF at a flow rate of 0.1 mL/min. van Deemter curves were constructed using flow rates from 0.05 to 1.4 mL/min (17 measurements) for the TITAN, BEH and HSS columns and from 0.05 to 1.2 mL/min (15 measurements) for the Cortecs columns, due to the increased pressure resulting from the smaller particle size. Diffusion coefficients were determined experimentally by the Taylor-Aris open tubular method using a flow rate of 0.1 mL/min and temperature controlled water

bath at 30 °C. The tubing used was PEEK with an internal diameter of 0.05277 cm, length of 303.1 cm, and coil diameter 22 cm. The Taylor-Aris measurements were verified using thiourea at 25 °C (Experiment  $1.32 \times 10^{-5} \text{ cm}^2/\text{s}$ , literature  $D_m = 1.33 \times 10^{-5} \text{ cm}^2/\text{s}$  [18,19]). Use of a longer tube did not appreciably affect the results. All measurements were performed at least in duplicate and were averaged.

### 3. Results and discussion

#### 3.1 Porosity comparison of different bare silica packed beds

Fig. 1 shows the inverse size exclusion chromatography (ISEC) plots for the four bare silica columns using a series of polystyrene standards eluted with neat THF. The external porosity ( $\epsilon_e$ ) was determined by extrapolation of the linear portion of the curve to zero MW. The total porosity ( $\epsilon_T$ ) of each column was determined from the elution volume of toluene in the HILIC mobile phase. As a control for  $\epsilon_e$  an Acquity 1.7  $\mu\text{m}$  BEH C18 50 mm x 2.1 mm column was included, which gave  $\epsilon_e = 0.354$ . This value compared very favourably to data obtained in a previous study [20]. Surprisingly, all of the fully porous bare silica packed columns gave much higher external porosities (0.410 to 0.438, see Fig. 1) than the reversed-phase (RP) column. For coreshell particles, it was shown by Guiochon *et al.* [21] that external porosities are usually higher than for those packed with fully porous materials, at least for RP columns. Guiochon *et al.* [12] also suggested that the topological structure of silica surfaces (roughness) can result in higher external porosity values. In their work, RP Zorbax (totally porous) and Halo (shell) particles both shared similar surface roughness characteristics and gave similarly higher external porosities (0.426 and 0.423 respectively) than for other totally porous RP packings. However this result is not indicated in Fig. 1, as the shell column gave a value similar to the totally porous columns (0.411). The unexpected results here could be due to differences in the packing processes used to pack bare silica materials.

It is known [22] that the internal particle porosity ( $\epsilon_{\text{int}}$ ) is significantly reduced upon chemical modification. This obviously has an impact on the total porosity of each column. The internal porosity ( $\epsilon_{\text{int}}$ ) of the core shell column shown in Fig. 1 was calculated according to ratio of the solid-core to the total particle diameter ( $\rho$ ) as follows [21]:

$$\epsilon_{\text{int}} = \frac{\epsilon_T - \epsilon_e}{(1 - \epsilon_e)(1 - \rho^3)} \quad (1)$$

(For the totally porous columns,  $\rho = 0$ ). The total porosity of the Cortecs column (0.549) was (as expected) around 15-25% lower than the fully porous particle packed columns (range 0.635-0.721).

This is similar to the observations of Zhang *et al.* [23] and Liekens *et al.* [14] when comparing HALO (core shell) and Acquity (fully porous) columns. Clearly, the Cortecs and TITAN columns have the lowest internal porosity ( $\epsilon_{\text{int}} = 0.357$  and  $0.367$  respectively), although the former (shell) column value was only slightly lower. The other totally porous BEH and HSS columns gave much larger values ( $\epsilon_{\text{int}} = 0.504$  and  $\epsilon_{\text{int}} = 0.456$  respectively). Liekens *et al.* [14] reported a correlation between internal porosity and pore size. Our results (compare Table 2) broadly support this correlation for the totally porous particles, but more data are needed for comparison.

### 3.2 Practical performance evaluation

Non-reduced van Deemter efficiency measurements ( $H$ - $u$  plots) remain important as they give a simple indication of what can be achieved by the practitioner. It is also useful to estimate the optimum achievable performance within the pressure limitations of current UHPLC instruments ( $\sim 1000$  bar). Figs. 2 (a) and (b) show the influence of increasing linear velocity on column pressure drop and on plate height (the latter using cytosine as a probe) respectively. The mobile phase compositions were adjusted to provide similar retention factors ( $k = 5.5$ - $6.0$ ) for cytosine at the respective optimum linear velocity for each column. In order to obtain a more realistic estimate of column performance, the five sigma peak width ( $5\sigma$ , PW at 4.4% of peak height) method was adopted. This method gives greater weight to tailing, which may be more severe at the base of the peak. Symmetrical peaks were obtained in all cases; asymmetry factors determined at 10% peak height were 1.14, 1.04, 1.01 and 0.93 for BEH, Cortecs, HSS and TITAN columns respectively. Corrections for extra-column band broadening were  $< 5\%$  in all cases due to the high  $k$  and 10 cm column format used. Table 2 summarises the (non-reduced)  $A$  (eddy dispersion),  $B$  (longitudinal diffusion) and  $C$  (resistance to mass transfer) fitting coefficients derived from the simple van Deemter equation, and the plate height  $H$  / column efficiency obtained at optimum flow. The decrease in the  $A$ -coefficient from  $2.2 \mu\text{m}$  for the TITAN column ( $d_p = 1.9 \mu\text{m}$ ) to  $1.3 \mu\text{m}$  for the Cortecs column ( $d_p = 1.6 \mu\text{m}$ ) is in agreement with expectations. However, relatively small differences in the  $B$ -coefficients are indicated in Table 2. The lowest  $C$ -coefficient was shown by the core-shell column. On average the  $1.6 \mu\text{m}$  Cortecs column gave a 33 % higher plate count than the fully porous columns, although at the expense of higher back pressure due to its smaller particle size. For instance, at  $300 \mu\text{L}/\text{min}$  (near the optimum linear flow of all the columns) the pressure drops were around 93, 100, 114 and 179 bar for the TITAN, HSS, BEH and Cortecs columns respectively. These figures indicate that optimum column performance in HILIC can be achieved using modest back pressures with all these 10 cm columns. As shown elsewhere [24] with still

smaller 1.3  $\mu\text{m}$  core-shell packed columns, the possibility to explore the high flow region is challenging due to instrument pressure limitations, at least with reversed-phase eluents.

In reduced coordinates, the minimum plate height ( $h$ ) of the 2.1 mm i.d. Cortecs column was 2.2 (Table 4). In contrast, reduced plate heights of 1.5 or lower have been obtained on larger particle (2.7  $\mu\text{m}$ ) silica shell particles packed in 4.6 mm i.d. formats, resulting in rather similar values of column efficiency in both cases [4]. Clearly, there are still some practical difficulties with the packing and operation of narrower bore and smaller particle shell columns for HILIC. Elsewhere, Fekete *et al.* [25] obtained  $h_{\text{min}} = 1.7$  for 50 mm x 2.1 mm ID Cortecs C18 1.6  $\mu\text{m}$   $d_p$  RP columns. Guiochon *et al.* [26] reported differences between different batches of Cortecs columns observing minimum reduced plate heights ( $h_{\text{min}}$ ) between 2.2-2.8 for 10 cm RP columns, similar to our values.

By using the approach of Desmet *et al.* [27] projection of column performance can be achieved by transforming non-reduced van Deemter data into so-called kinetic plots. Figs. 3 (a) and (b) show two simple representations of the data. Table 3 shows the viscosity, flow resistance and permeability parameters for each column. The viscosity changes of the mobile phases are small (0.39-0.41 cP) for the small range of acetonitrile compositions used (90.1-93.7 %); thus this factor should not greatly influence the kinetic plots. Considering the region of practical relevance (3,000-100,000 theoretical plates,  $N$ ) and a maximum pressure drop  $\Delta P=1000$  bar, Fig. 3 (a) shows that the Cortecs column outperforms all the other columns. In the fast analysis region ( $t_0 \leq 20$  s) the divergence becomes more marked between the Cortecs column and the fully porous types. For instance, at  $t_0 = 10$  s the plate counts were projected to be approximately 23,000, 14,000, 14,000 and 12,000 for the Cortecs, BEH, HSS and TITAN columns respectively. Clearly, the differences in performance here are due to the inherently higher efficiency of Cortecs particles and the lower  $C$ -coefficient as observed in Fig. 1 (b). Note these projections pertain to operation at 1000 bar and as such, compressibility and changes in viscosity of the acetonitrile-rich mobile phases used could affect the accuracy of predictions. Fig. 3 (b) is another useful kinetic plot transformation, where the minimum of each curve pertains to the optimum column length operated at the pressure maximum of the system. This figure mirrors that of a typical van Deemter curve with a  $B$ - and  $C$ -term regions except that each point on the curve represents a column of fixed length, operated at the maximum pressure of the system. The minimum of each curve relates to the separation impedance ( $E$ ) by the following equation [28]:



$$E = \frac{\Delta P_{\max}}{\eta} \frac{t_0}{N^2} = h^2 \Phi \quad (2)$$

The value of  $E$  is a dimensionless figure of merit which describes the compromise between efficiency, speed and pressure. Calculated values of  $E$  were 2200, 2900, 3100 and 2800 for the Cortecs, BEH, HSS and TITAN columns respectively. The low value for the Cortecs column emphasises the significant performance gains of this column relative to fully porous particle packed columns within the pressure capabilities of a typical UHPLC instrument. As depicted in Fig. 3 (b), the  $E$  value obtained for the Cortecs column is attained at a lower  $N$  value in comparison with the other columns due to the smaller particle size of this phase (1.6  $\mu\text{m}$ ).

### 3.3 Arrested elution and reduced van Deemter analysis

In order to investigate further the reasons for the similar  $B$ -coefficients observed in the non-reduced van Deemter curve analysis, arrested elution measurements were performed. We extended the analysis to include nortriptyline as well as cytosine, as nortriptyline may be retained by mostly ionic processes rather than pure hydrophilic processes. Arrested elution involves stopping the flow for a series of increasing parking times ( $t_{\text{park}}$ ) once the analyte has migrated about half-way down the column. After each park time, the flow is resumed, the analyte band is eluted from the column and the peak variance is measured. The additional peak broadening that takes place in the parking period is given by [14,29]

$$\sigma_z^2 = 2 D_{\text{eff}} \cdot t_{\text{park}} \quad (3)$$

where  $\sigma_z$  is measured in units of column length.

$$\sigma_z^2 = \sigma_t^2 \cdot u^2 \quad (4)$$

where  $u$  is the linear flow velocity and  $\sigma_t$  is measured in units of time. Thus:

$$\sigma_t^2 = 2 D_{\text{eff}} \cdot t_{\text{park}} / u^2 \quad (5)$$

$D_{\text{eff}}$  can be determined from a plot of  $\sigma_t^2$  against  $t_{\text{park}}$ . The intercept of these plots is due to the normal band broadening processes that take place during flow of the solute through the column, and includes extra-column band broadening.

The non-reduced B coefficient can be calculated [29] from (6)

$$B = 2D_{eff}(1+k) \quad (6)$$

The reduced  $b$ -coefficient can then be determined from (7) if the bulk mobile phase diffusion coefficient ( $D_m$ ) is known:

$$b = 2 \frac{D_{eff}}{D_m} (1+k) \quad (7)$$

Fig. 4 shows data for the arrested elution experiment performed using nortriptyline on each column. Excellent linearity was observed in all experiments with  $r^2 > 0.999$  being obtained in each case. Table 4 summarises data from the arrested elution experiments performed on each column for cytosine and nortriptyline and from curve fitting of reduced van Deemter plots (Fig. 5). Reduced van Deemter data (Figs. 5 (a) and (b)) were plotted as:

$$v = \frac{u \cdot d_p}{D_m} \quad (8a)$$

$$h = \frac{H}{d_p} \quad (8b)$$

As shown elsewhere [27,36], the low  $b$ -coefficient in HILIC compared with RP can be mainly attributed to the reduced surface diffusion contributions due to elements of localisation in the retention mechanism and the presence of a water layer on the column surface, which restricts surface diffusion. Interestingly, Table 4 indicates that the particle morphology has only a small influence on the axial diffusion behaviour in HILIC, as shown by the rather similar reduced  $b$ -coefficients (range 2.04-2.37) for cytosine on the 4 columns from arrested elution experiments. The range of  $b$ -coefficients for nortriptyline is also small (3.39-3.85) with Cortecs having for this solute < 10% lower value than the average of the totally porous particles. Both Liekens *et al.* [14] and Guiochon *et al.* [15] showed that core-shell particles offer substantially lower axial diffusion contributions (20-40%) compared with fully porous particle in RP chromatography. Interestingly, our results show an appreciable difference between the effective diffusion behaviours of cytosine and nortriptyline. On average,  $D_{eff}/D_m$  for nortriptyline was around 40% larger than for cytosine. In particular, the ratio  $D_{eff}/D_m$  for nortriptyline is almost double that for cytosine on the BEH column. This indicates that the diffusion experienced inside the column is much greater for nortriptyline. We

speculate that nortriptyline, which is retained mostly by ion-exchange and is relatively hydrophobic, explores a more acetonitrile-rich zone in the pore volume. In contrast, cytosine is more hydrophilic and may be retained mostly by partition into the aqueous rich zone held close to the surface of the pore wall. As shown in Fig. 5 (b) the reduced van Deemter curve for nortriptyline on BEH is very different to that obtained for cytosine on the same phase, as indicated by the higher  $b$ -coefficient and lower  $c$ -coefficient for nortriptyline. Fig. 5 (a) shows the reduced van Deemter curves for cytosine on each of the columns. Table 4 indicates that there are clear differences in the performance and in the  $c$ -coefficient behaviour of each phase. In particular, the BEH column showed the largest  $c$ -coefficient for cytosine which might be attributed to the hybrid material structure or due to frictional heating effects. For instance, hybrid silica has been reported to have distinctly lower thermal conductivity than conventional silicas and core-shell materials [15]. Frictional heating may be emphasised as the mobile phase used is mostly acetonitrile, which in turn also has low thermal conductivity compared with highly aqueous eluents [20]. The combined effect may influence radial long-range eddy diffusion equilibrium within the column. The  $c$ -coefficient for nortriptyline on the BEH particle contradicts this argument somewhat, however the faster diffusion kinetics inside the particle may counteract the negative effects of frictional heating (See section 3.4).

### 3.4 Maxwell-EMT (Effective Medium Theory) analysis to determine intra-particle diffusion ( $D_{part}$ )

Using the ratio  $\gamma_{eff} = D_{eff}/D_m$  obtained from arrested elution and bulk diffusion coefficient measurements, it is possible to derive the intra-particle diffusion experienced by an analyte. The  $D_{part}$  term is a measure of the analyte diffusion inside the particle porous structure independent of that experienced in the interstitial space. The use of Maxwell-EMT expressions have been discussed in detail by Desmet *et al.* [13,33] for investigating  $B$ -coefficient behaviour in packed columns. Firstly, the so-called polarizability constant ( $\beta_1$ ) must be derived and subsequent calculation of the  $\alpha_{part}$  as follows:

$$\beta_1 = \frac{1}{1 - \varepsilon_e} \cdot \frac{\gamma_{eff} \varepsilon_T (1 + k) - 1}{2 + \gamma_{eff} \varepsilon_T (1 + k)} \quad (9)$$

$$\alpha_{part} = \frac{1 + 2\beta_1}{1 - \beta_1} \quad (10)$$

$$\frac{D_{part}}{D_m} = \frac{\alpha_{part}(1 - \varepsilon_e)}{\varepsilon_T(1 + k) - \varepsilon_e} \quad (11)$$

The  $\alpha_{part}$  corresponds to the flux in chemical potential and associated gradient with respect to analyte transport from the bulk mobile phase to the partitioned state. Furthermore, for shell particles, correction to  $D_{part}$  due to the presence of the impermeable solid core can be made. This affords determination of solute diffusion in only the porous region of the shell ( $D_{pz}$ ) as follows:

$$\frac{D_{part}}{D_{pz}} = \frac{2}{2 + \rho^3} \quad (12)$$

Clearly, for fully porous particles where there is no solid core present,  $\rho = 0$  and  $D_{part} = D_{pz}$ . Using  $D_{pz}/D_m$  values allow for examination of the physical diffusion processes occurring in the meso-pores of the stationary phase. Fig. 6 shows the calculated  $D_{pz}/D_m$  ratios for cytosine and nortriptyline for the different particle types. Notably, there are no dramatic differences in  $D_{pz}/D_m$  for either cytosine or nortriptyline when comparing the values for a given solute on the different columns. The subtle variations can be explained by the differing mesoporous structure of the silica particles; an inherent function of the particle synthesis. The influence of the solid-core on solute diffusion with the Cortecs column is not apparent for either solute. This can be explained due to the low  $D_{pz}/D_m$  values obtained in the HILIC mode as the contribution of surface diffusion is much smaller compared to RP. As shown by the theoretical calculations made by Deridder *et al.* [13], the presence of a solid-core is indeed predicted to be negligible in reducing the  $b$ -coefficient when  $D_{pz}/D_m$  values are small (e.g. 0.1); the values for nortriptyline and cytosine (Fig. 6) are of this order. As discussed in [13], the larger the core, the more the effective diffusion through the particle is reduced. However, the obstructing effect of the solid core is more pronounced when the diffusion rate in the meso-porous zone is large. Conversely, when this rate is small, the dominant diffusion trajectory will be in the interstitial void space where the diffusion is much faster. There remain clear differences between  $D_{pz}/D_m$  values when comparing nortriptyline with cytosine. The values indicate that nortriptyline experiences much faster diffusion inside the particle, which can be used to explain the larger  $b$ -coefficient and lower  $c$ -term values obtained for this solute compared with cytosine (Fig. 5). This finding adds some weight

to the speculation that nortriptyline could be transported through the particle in a faster diffusion zone (acetonitrile-rich) inside the pore volume. In contrast, cytosine perhaps explores the more water-rich zone nearer the pore wall, which results in correspondingly slower diffusion (due to the potentially higher micro-viscosity of the water layer).

In order to expand the study further, concentrating on the BEH column only, arrested elution data were obtained for a selection of ionogenic solutes with distribution coefficients ( $\log D_w^{\text{pH } 3}$ ) ranging from -2.8 – 1.1 and different molecular weights. Fig. 7 and Table 5 show these data for the solutes with conditions adjusted to yield similar high retention factors ( $k = 5.5-6.0$ ) as previously, with data for cytosine and nortriptyline also included. Fig. 8 shows the  $D_{\text{part}}/D_m$  values for each solute plotted against  $\log D_w^{\text{pH } 3}$  indicating a moderate positive linear association ( $R = 0.8$ ). Clear differences in the diffusion rate inside the particles for the different ionogenic solutes were obtained. These data again suggest that the aqueous solubility (relative interaction with the water layer) of each solute perhaps influences the  $b$ -coefficient. For instance, benzylamine and cytosine have similar negative  $\log D$  values and showed similar low  $b$ -coefficients as reflected by their  $D_{\text{part}}/D_m$  ratios. In contrast, diphenhydramine and nortriptyline, which are considerably more hydrophobic, having the highest  $\log D$  values, showed similarly larger  $b$ -coefficients and  $D_{\text{part}}/D_m$  ratios. Nevertheless, Fig. 8 shows that the points for cytosine, benzylamine and phenylephrine show scatter about the regression line. The relative contributions of ion-exchange and partitioning each solute experiences could also be influential, as well as complex solvation effects arising from the structural properties of the analyte. There is also likely to be a degree of error due to the  $\log D$  predictions used. Overall, this trend should be considered in practical applications, as the optimum linear velocity for each solute will consequently be different. A further consequence is that the  $c$ -term (high linear velocity) region will be affected when considering fast analysis applications, due to the different diffusion rates inside the particle e.g. for cytosine versus nortriptyline.

In summary, the  $b$ -coefficient should not be expected to be closely similar for different ionogenic solutes at fixed, appreciable retention factors  $k > 5$  in HILIC. This has practical implications (flow optimisation) for when the technique is applied to a wide range of analytes with different physiochemical properties. Additionally, there appears to be little influence of the core-shell morphology in reducing the  $b$ -coefficients under HILIC conditions. Nevertheless, the choice of bare silica as a HILIC phase should be based on other factors including optimisation of peak shape and retentivity (See section 3.5).

### 3.5 Evolution of retention and peak shape with buffer concentration

In order to compare the ranges of retentivity and peak symmetry achievable with each bare silica phase the effect of varying buffer concentration at fixed acetonitrile concentration was performed. As a comparator, an amide functionalised HILIC column was introduced to the study. We used a test mix comprising the weak hydrophilic base cytosine, the stronger bases procainamide (hydrophilic) and nortriptyline (hydrophobic) and the two neutral hydrophilic compounds 5-(Hydroxymethyl)uridine and uracil. We specifically chose uracil as it has a similar structure to 5-(Hydroxymethyl)uridine but does not possess the extensive hydroxylation caused by the pentose moiety. Plots of  $k$  versus  $1/[M^+]$  as per Cox and Stout [34] can be used to estimate the degree of ionic retention. Fig. 9 shows such plots determined for the bare silica columns (94.8 % ACN containing 1.1-8.4 mM overall ammonium formate  $w^w$  pH 3). Fig. 10 shows the same experiment performed on the hybrid BEH silica and BEH Amide hybrid silica columns. For the (non-hybrid) bare silica columns, the neutral solutes uracil, 5-(Hydroxymethyluridine) and pseudo-neutral compound (cytosine) showed increases in  $k$  with increasing buffer concentration, with the largest effect for 5-(Hydroxymethyluridine) which has the lowest logP (-2.61 average value from ACD/Marvin/MedChem Designer). The increase in  $k$  for the neutral solutes with increasing buffer concentrations might be attributable to the formation of a thicker water layer, resulting in increased partitioning. This result is also shown with the BEH Amide phase (Fig. 10). Much larger *decreases* in  $k$  were obtained for the ionised solutes nortriptyline and procainamide. For the ionogenic compounds, the plots are curved, similar to that found in a previous study [35]. This could be due to a small degree of ion pairing with formate anions in the acetonitrile-rich mobile phase. The curvature precludes accurate estimation of the % of ion-exchange contributions to  $k$ , but extrapolation of the plots to infinite buffer concentration indicates a high proportion of the retention is attributable to ion exchange for these basic solutes on all columns. Nevertheless, the absolute magnitude of ionic retention differs substantially between the columns at a given buffer concentration, with particularly high  $k$  values shown for the bases at low buffer concentration on the TITAN column while low values were obtained using the BEH column.

Figs. 9 and 10 also show the variation in peak asymmetry (10% height) with increasing buffer concentration. It is notable that the asymmetry of basic compounds is hardly affected by buffer strength on any of the bare silica columns, including the TITAN column. Indeed, these compounds together with cytosine and uracil gave asymmetries within an acceptable range of 0.9-1.3 even at low buffer concentrations. This result is favourable for electrospray ionisation mass spectrometry where sensitivity is improved at low buffer concentration. In contrast, is the deterioration in peak

shape for (neutral) 5-(hydroxymethyl)uridine with decreasing buffer concentration, especially for the TITAN and Cortecs phases. A feature of this compound is the presence of the pentose conjugate which has three hydroxyl groups. It is conceivable that with decreasing buffer concentration, surface heterogeneity becomes less shielded, promoting multi-point hydrogen bonding [36] interactions between hydroxyl and silanol groups. Possibly, at elevated buffer concentrations, partition dominates the retention mechanism rather than direct silanol hydrogen bonding interactions. In contrast, the same behaviour was absent with the BEH Amide phase, where access to silanol groups is potentially minimised by the presence of the bonded group. Lastly, the basic compounds showed progressively worse peak shape at lower buffer concentrations on the BEH Amide. We speculate that this may be due to overloading of a smaller number of high energy active sites within the underlying silica on this phase.

To summarise, further work is required to elucidate the curvature of the plots of  $k$  versus  $1/[M^+]$  and to perform experiments at different % organic. It may be possible that the balance of partition and ionic processes differ in less organic rich mobile phases than used here. It is also important to investigate further the dependence on buffer-type and concentration in obtaining satisfactory peak shape for hydroxylated compounds on bare silica.

#### 4. Conclusion

The kinetic performance of a sub-2  $\mu\text{m}$  bare silica core shell column was shown to be improved compared with totally porous columns of the same internal diameter (2.1 mm) in the HILIC mode. Nevertheless, minimum reduced plate heights were greater than found previously for sub-3  $\mu\text{m}$  core shell 4.6 mm ID silica columns, indicating that problems with the packing and operation of narrower and smaller particle size columns still exist. The external porosity of fully porous bare silica HILIC columns was shown to be higher than expected when compared with both literature values and a control RP column. The absence of chemical modification and different packing methods may explain this variation. Only small differences were observed in reduced  $b$ - and  $B$ -coefficients for the same solute between the different particle morphologies in the HILIC mode. The merits of the core-shell column may be attributed to superior bed homogeneity that reduces the van Deemter  $a$ - and  $A$ - coefficients, and possibly also to improved thermal conductivity of the material, which reduces the apparent  $c$ - and  $C$ - coefficients. Differences in kinetic performance of a charged hydrophobic base (nortriptyline) and weak hydrophilic base (cytosine) were seen in terms of the diffusion inside the particles ( $D_{\text{part}}$ ), which was considerably greater for the former solute. It is possible that this

increased diffusion of hydrophobic bases results from their retention in a more acetonitrile-rich region inside the pores compared with that of more hydrophilic solutes. The retention of ionised bases decreased substantially over the concentration range 1.1-8.4 mM typically favoured for mass spectrometry applications, indicating ionic interactions. However, the peak shape for these substances was hardly affected. While similar results were obtained for neutral compounds, the multiply hydroxylated solute 5-(hydroxymethyl uridine) gave poor peak shape at low buffer concentrations, which may possibly be related to strong adsorption under these conditions.

#### Acknowledgements

This work was supported by the United Kingdom Engineering and Physical Sciences Research Council [grant number EP/J016578/1].



## References

- [1] A.J. Alpert, Hydrophilic-interaction chromatography for the separation of peptides, nucleic acids and other polar compounds., *J. Chromatogr.* 499 (1990) 177–96.
- [2] D. V McCalley, Is hydrophilic interaction chromatography with silica columns a viable alternative to reversed-phase liquid chromatography for the analysis of ionisable compounds?, *J. Chromatogr. A.* 1171 (2007) 46–55.
- [3] D. V McCalley, The challenges of the analysis of basic compounds by high performance liquid chromatography: some possible approaches for improved separations., *J. Chromatogr. A.* 1217 (2010) 858–80.
- [4] D. V McCalley, Evaluation of the properties of a superficially porous silica stationary phase in hydrophilic interaction chromatography., *J. Chromatogr. A.* 1193 (2008) 85–91.
- [5] C.G. Horvath, B.A. Preiss, S.R. Lipsky, Fast liquid chromatography. Investigation of operating parameters and the separation of nucleotides on pellicular ion exchangers, *Anal. Chem.* 39 (1967) 1422–1428.
- [6] J.J. Kirkland, Controlled surface porosity supports for high-speed gas and liquid chromatography, *Anal. Chem.* 41 (1969) 218–220.
- [7] J.M. Cunliffe, T.D. Maloney, Fused-core particle technology as an alternative to sub-2-microm particles to achieve high separation efficiency with low backpressure., *J. Sep. Sci.* 30 (2007) 3104–9.
- [8] D. V McCalley, Instrumental considerations for the effective operation of short, highly efficient fused-core columns. Investigation of performance at high flow rates and elevated temperatures., *J. Chromatogr. A.* 1217 (2010) 4561–7.
- [9] D. Cabooter, A. Fanigliulo, G. Bellazzi, B. Allieri, A. Rottigni, G. Desmet, Relationship between the particle size distribution of commercial fully porous and superficially porous high-performance liquid chromatography column packings and their chromatographic performance., *J. Chromatogr. A.* 1217 (2010) 7074–81.
- [10] F. Gritti, G. Guiochon, Comparison of heat friction effects in narrow-bore columns packed with core-shell and totally porous particles, *Chem. Eng. Sci.* 65 (2010) 6310–6319.
- [11] L.E. Blue, J.W. Jorgenson, 1.1  $\mu\text{m}$  superficially porous particles for liquid chromatography. Part I: synthesis and particle structure characterization., *J. Chromatogr. A.* 1218 (2011) 7989–95.
- [12] F. Gritti, G. Guiochon, Comparative study of the performance of columns packed with several new fine silica particles. Would the external roughness of the particles affect column properties?, *J. Chromatogr. A.* 1166 (2007) 30–46.
- [13] S. Deridder, G. Desmet, Effective medium theory expressions for the effective diffusion in chromatographic beds filled with porous, non-porous and porous-shell particles and cylinders. Part II: Numerical verification and quantitative effect of solid core on expected B-term band, *J. Chromatogr. A.* 1218 (2011) 46–56.

- [14] A. Liekens, J. Denayer, G. Desmet, Experimental investigation of the difference in B-term dominated band broadening between fully porous and porous-shell particles for liquid chromatography using the Effective Medium Theory., *J. Chromatogr. A.* 1218 (2011) 4406–16.
- [15] F. Gritti, G. Guiochon, Mass transfer resistance in narrow-bore columns packed with 1.7 microm particles in very high pressure liquid chromatography., *J. Chromatogr. A.* 1217 (2010) 5069–83.
- [16] K.D. Wyndham, J.E. O’Gara, T.H. Walter, K.H. Glose, N.L. Lawrence, B.A. Alden, et al., Characterization and evaluation of C18 HPLC stationary phases based on ethyl-bridged hybrid organic/inorganic particles., *Anal. Chem.* 75 (2003) 6781–8.
- [17] A. Kumar, J.C. Heaton, D. V McCalley, Practical investigation of the factors that affect the selectivity in hydrophilic interaction chromatography., *J. Chromatogr. A.* 1276 (2013) 33–46.
- [18] D.B. Ludlum, R.C. Warner, H.W. Smith, The diffusion of thiourea in water at 25 °C, *J. Phys. Chem.* 66 (1962) 1540–1542.
- [19] P.J. Dunlop, C.N. Pepela, B.J. Steel, Diffusion study at 25.deg. with a shearing diffusimeter. Comparison with the Gouy and conductance methods, *J. Am. Chem. Soc.* 92 (1970) 6743–6750.
- [20] D. V McCalley, Some practical comparisons of the efficiency and overloading behaviour of sub-2 µm porous and sub-3 µm shell particles in reversed-phase liquid chromatography., *J. Chromatogr. A.* 1218 (2011) 2887–97.
- [21] F. Gritti, A. Cavazzini, N. Marchetti, G. Guiochon, Comparison between the efficiencies of columns packed with fully and partially porous C18-bonded silica materials., *J. Chromatogr. A.* 1157 (2007) 289–303.
- [22] F. Gritti, G. Guiochon, General HETP equation for the study of mass-transfer mechanisms in RPLC., *Anal. Chem.* 78 (2006) 5329–47.
- [23] Y. Zhang, X. Wang, P. Mukherjee, P. Petersson, Critical comparison of performances of superficially porous particles and sub-2 microm particles under optimized ultra-high pressure conditions., *J. Chromatogr. A.* 1216 (2009) 4597–605.
- [24] S. Fekete, D. Guillarme, Kinetic evaluation of new generation of column packed with 1.3 µm core-shell particles., *J. Chromatogr. A.* 1308 (2013) 104–13.
- [25] B. Bobály, D. Guillarme, S. Fekete, Systematic comparison of a new generation of columns packed with sub-2 µm superficially porous particles., *J. Sep. Sci.* 37 (2014) 189–97.
- [26] F. Gritti, S.J. Shiner, J.N. Fairchild, G. Guiochon, Evaluation of the kinetic performance of new prototype 2.1×100mm narrow-bore columns packed with 1.6µm superficially porous particles, *J. Chromatogr. A.* 1334 (2014) 30–43.
- [27] G. Desmet, D. Clicq, P. Gzil, Geometry-independent plate height representation methods for the direct comparison of the kinetic performance of LC supports with a different size or morphology., *Anal. Chem.* 77 (2005) 4058–70.

- [28] D. Cabooter, J. Billen, H. Terry, F. Lynen, P. Sandra, G. Desmet, Kinetic plot and particle size distribution analysis to discuss the performance limits of sub-2 micron and supra-2 micron particle columns., *J. Chromatogr. A.* 1204 (2008) 1–10.
- [29] J.H. Knox, H.P. Scott, B and C terms in the Van Deemter equation for liquid chromatography, *J. Chromatogr. A.* 282 (1983) 297–313.
- [30] F. Gritti, G. Guiochon, Mass transfer mechanism in hydrophilic interaction chromatography., *J. Chromatogr. A.* 1302 (2013) 55–64.
- [31] F. Gritti, G. Guiochon, Comparison between the intra-particle diffusivity in the hydrophilic interaction chromatography and reversed phase liquid chromatography modes. Impact on the column efficiency., *J. Chromatogr. A.* 1297 (2013) 85–95.
- [32] J.C. Heaton, X. Wang, W.E. Barber, S.M.C. Buckenmaier, D. V McCalley, Practical observations on the performance of bare silica in hydrophilic interaction compared with C18 reversed-phase liquid chromatography., *J. Chromatogr. A.* 1328 (2014) 7–15.
- [33] G. Desmet, S. Deridder, Effective medium theory expressions for the effective diffusion in chromatographic beds filled with porous, non-porous and porous-shell particles and cylinders. Part I: Theory., *J. Chromatogr. A.* 1218 (2011) 32–45.
- [34] G.B. Cox, R.W. Stout, Study of the retention mechanism for basic compounds on silica under “pseudo-reversed-phase” conditions, *J. Chromatogr. A.* 384 (1987) 315–336.
- [35] D. V McCalley, Study of the selectivity, retention mechanisms and performance of alternative silica-based stationary phases for separation of ionised solutes in hydrophilic interaction chromatography., *J. Chromatogr. A.* 1217 (2010) 3408–17.
- [36] N.P. Dinh, T. Jonsson, K. Irgum, Probing the interaction mode in hydrophilic interaction chromatography., *J. Chromatogr. A.* 1218 (2011) 5880–91.
- [37] H. Chen, C. Horvath, Rapid separation of proteins by reversed phase HPLC at elevated temperatures., *Anal. Methods Instrum.*, 1 (1993) 213-222.

## Legend to Figures

Fig. 1 Inverse size exclusion chromatography (ISEC) for each column. The (**x**) denotes the  $MW^{1/3}$  versus  $V_r$  ( $\text{cm}^3$ ) for toluene.

Fig. 2 (a) Linear velocity versus corrected columns pressure drop (b) non-reduced van Deemter plot of linear velocity versus height equivalent to a theoretic plate.

Fig. 3 (a) Kinetic plot of  $t_o$  versus  $N$  and (b)  $t_o/N^2$  versus  $N$  for each column. Same symbols as in Figure 2.

Fig. 4 Arrested elution plots for nortriptyline on each column.

Fig. 5 (a) Reduced van Deemter plot for BEH/Cortecs/HSS/TITAN using cytosine as the test solute and (b) for BEH HILIC comparing cytosine (closed symbols) and nortriptyline (open symbols). Symbols for (a) as in Figure 2.

Fig. 6 Comparison of  $D_{pz}/D_m$  for each column derived from Maxwell-EMT calculations using cytosine and nortriptyline.

Fig. 7 Arrested elution plots for different ionogenic solutes on BEH HILIC.

Fig. 8 Plot of  $D_{pz}/D_m$  for different ionogenic solutes derived from Maxwell-EMT calculations versus  $\log D_w^w \text{pH}3$ .

Fig. 9 Plot of  $k$  (top) and  $As_{0.1}$  (bottom) versus  $1/[M^+]$  using a mobile phase of 94.8% ACN containing 1.1-8.4 mM overall ammonium formate  $w^w \text{pH} 3$  for Cortecs/HSS/TITAN bare silica columns.

Fig. 10 Plot of  $k$  (top) and  $As_{0.1}$  (bottom) versus  $1/[M^+]$  using a mobile phase of 94.8% ACN containing 1.1-8.4 mM overall ammonium formate  $w^w \text{pH} 3$  for BEH HILIC and BEH Amide columns.

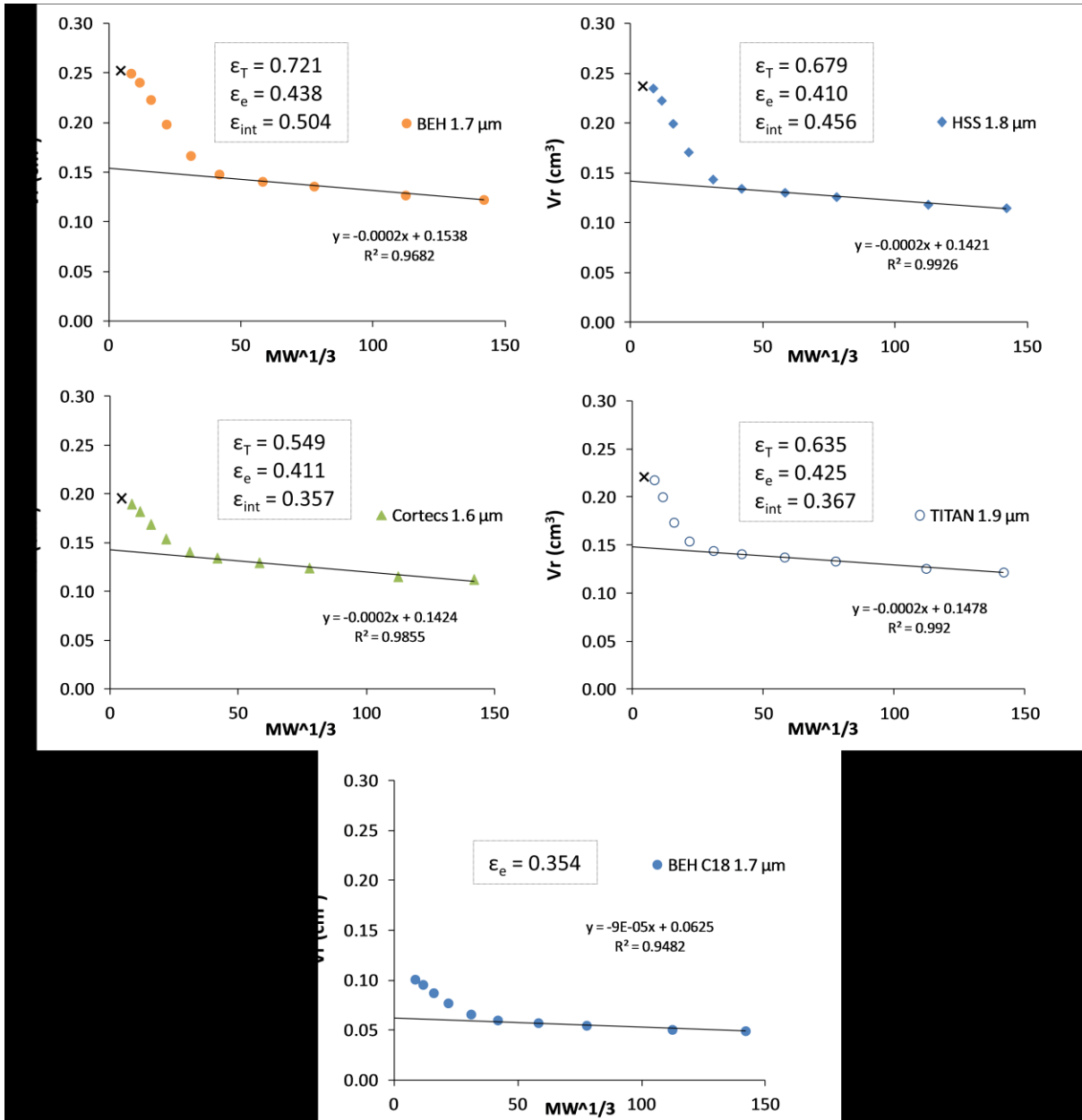
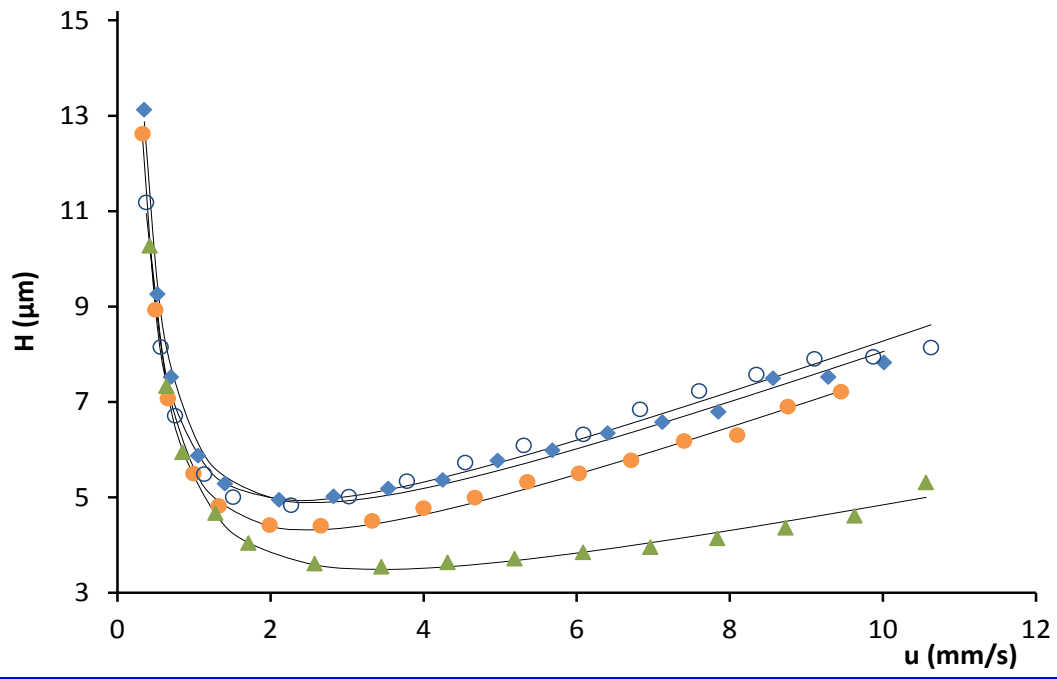
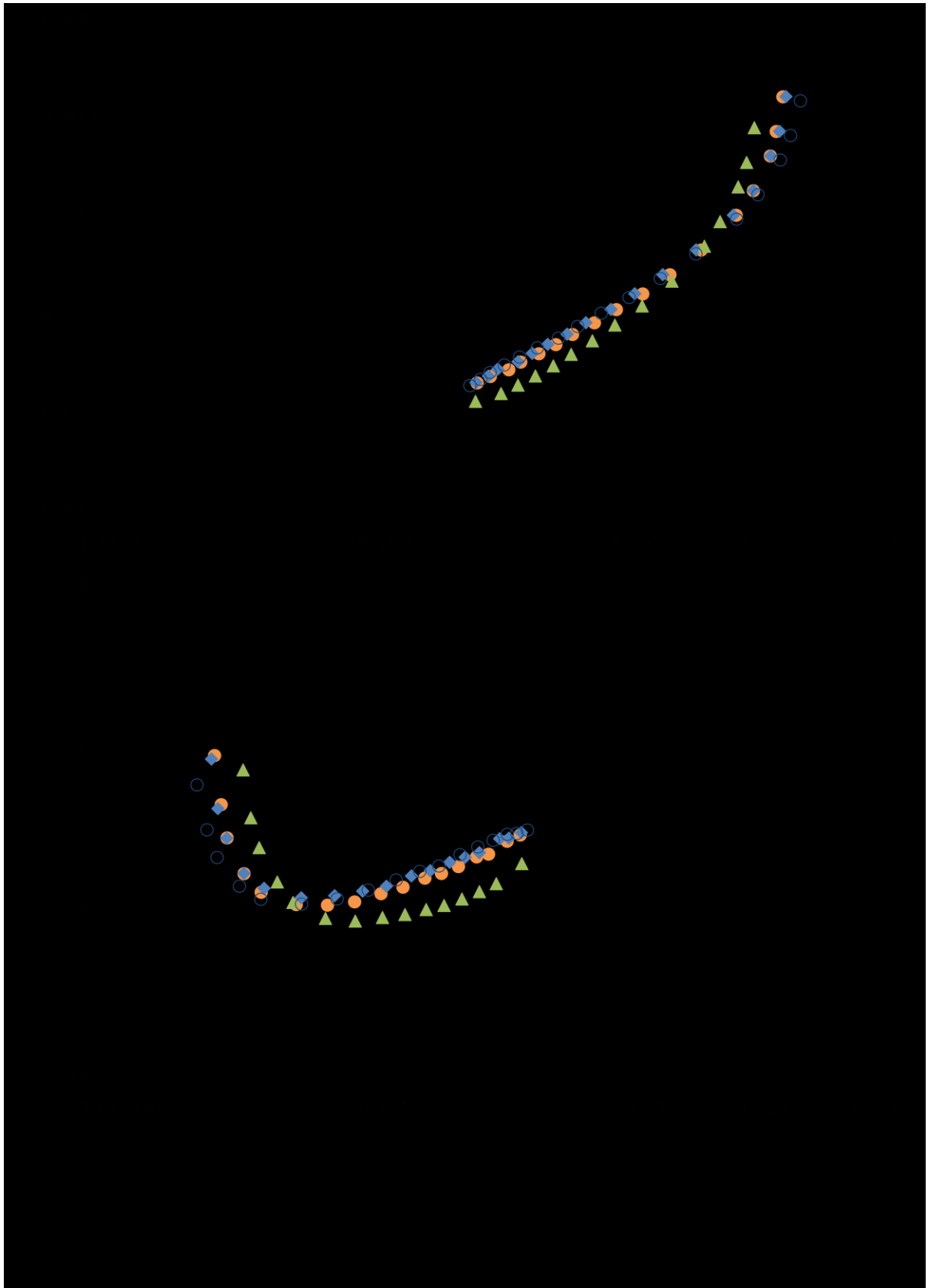
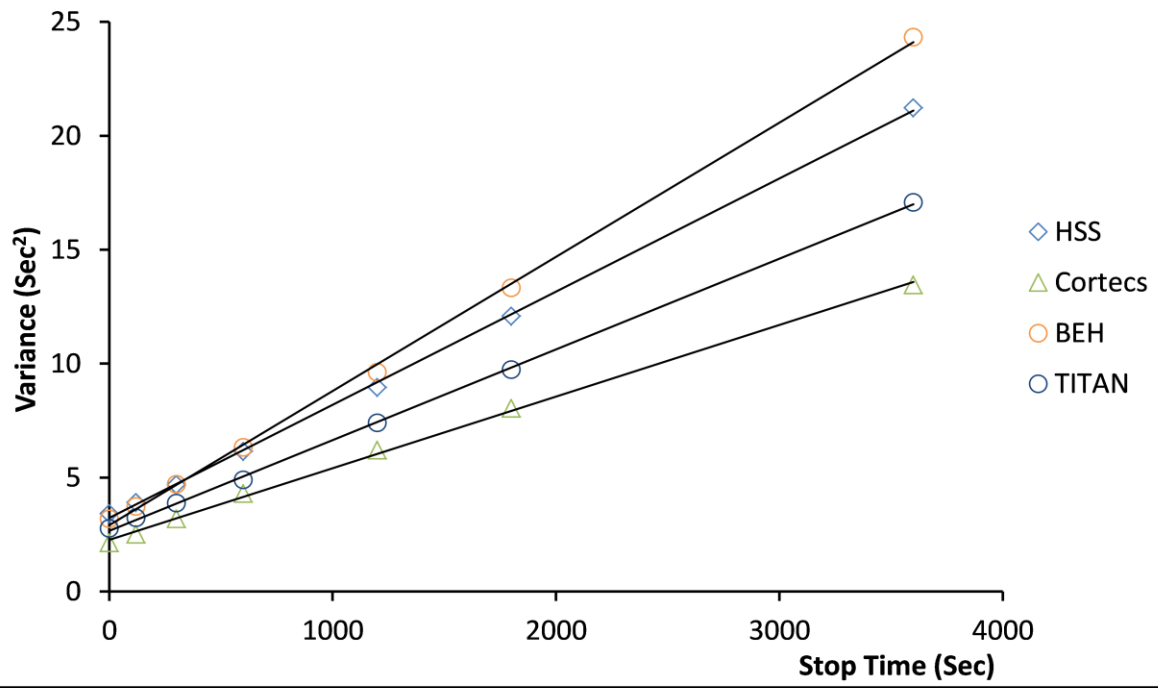


Fig 1

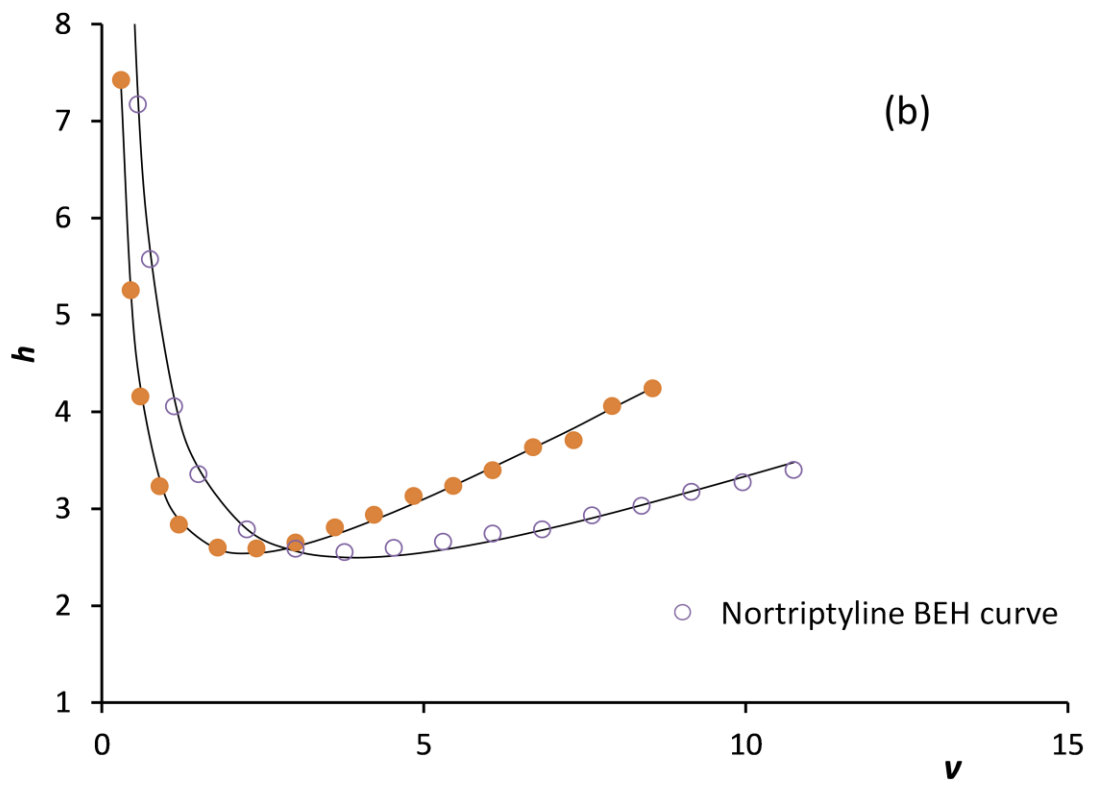
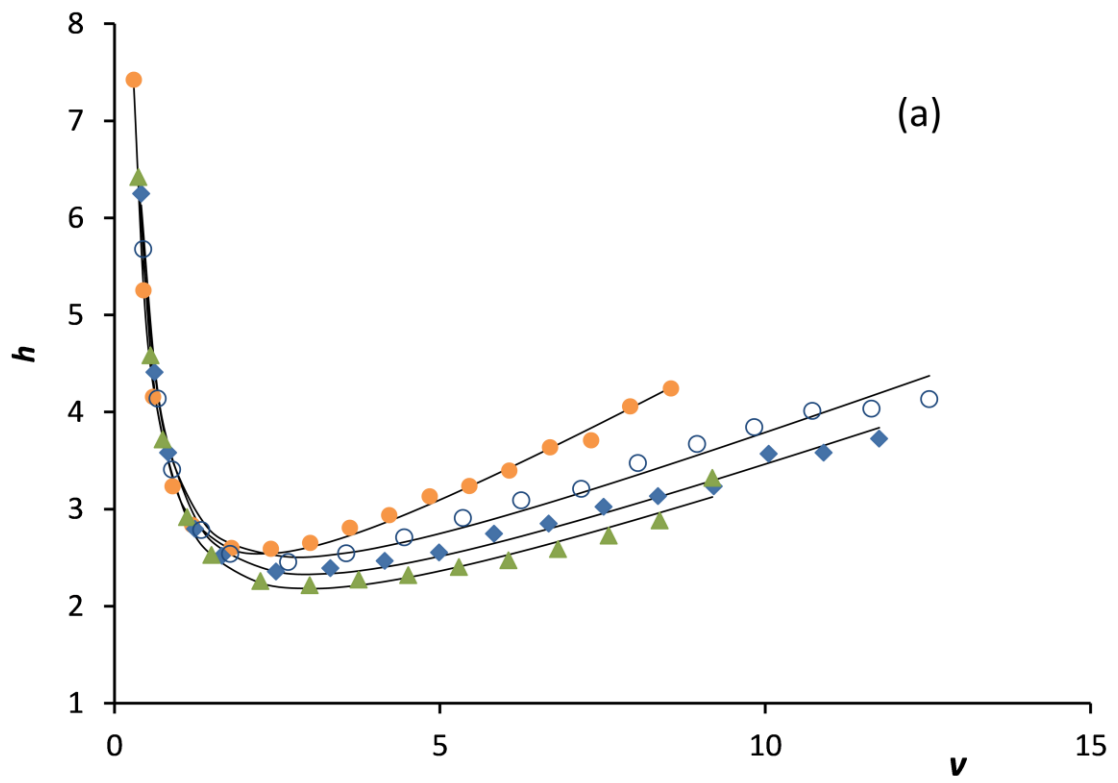


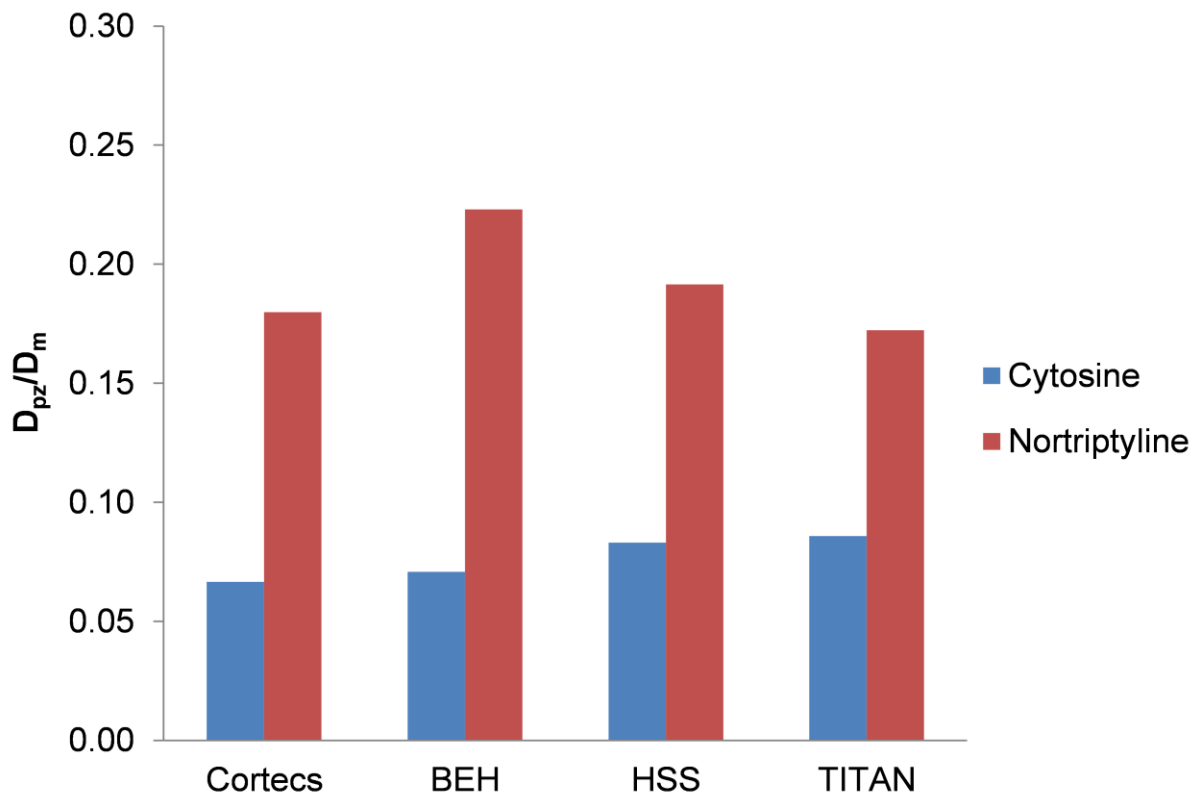
● BEH 1.7 µm    ◆ HSS 1.8 µm    ▲ Cortecs 1.6 µm    ○ TITAN 1.9 µm    [Fig 2](#)

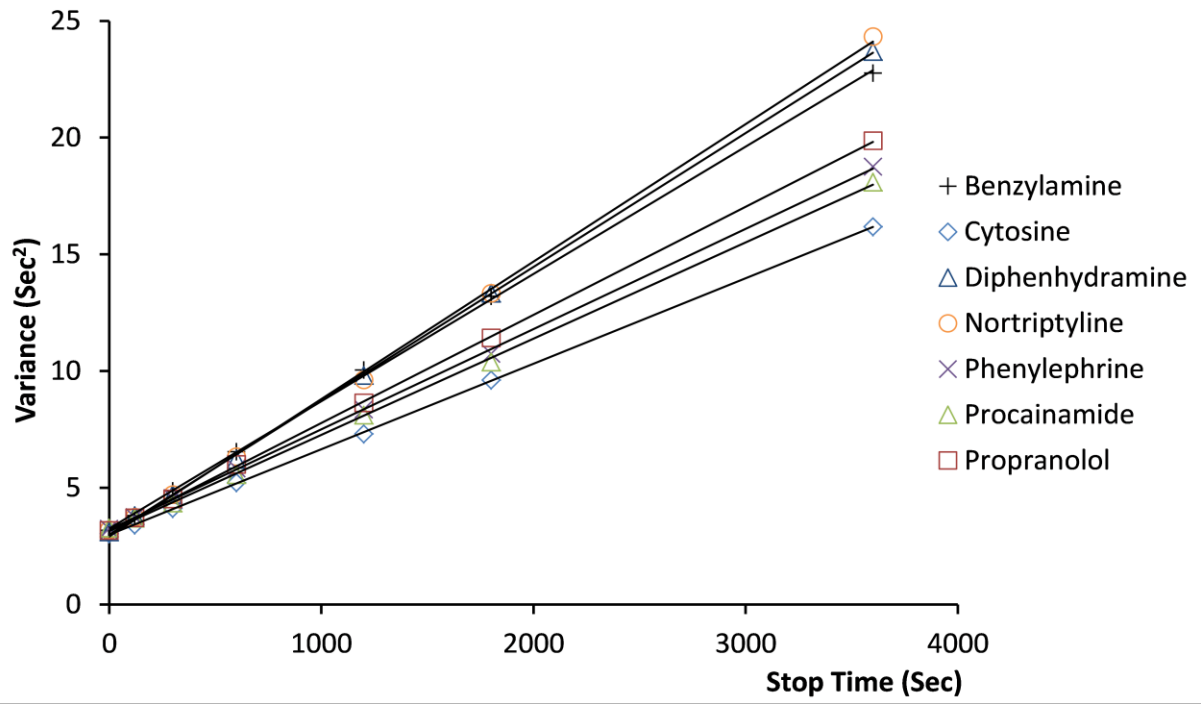


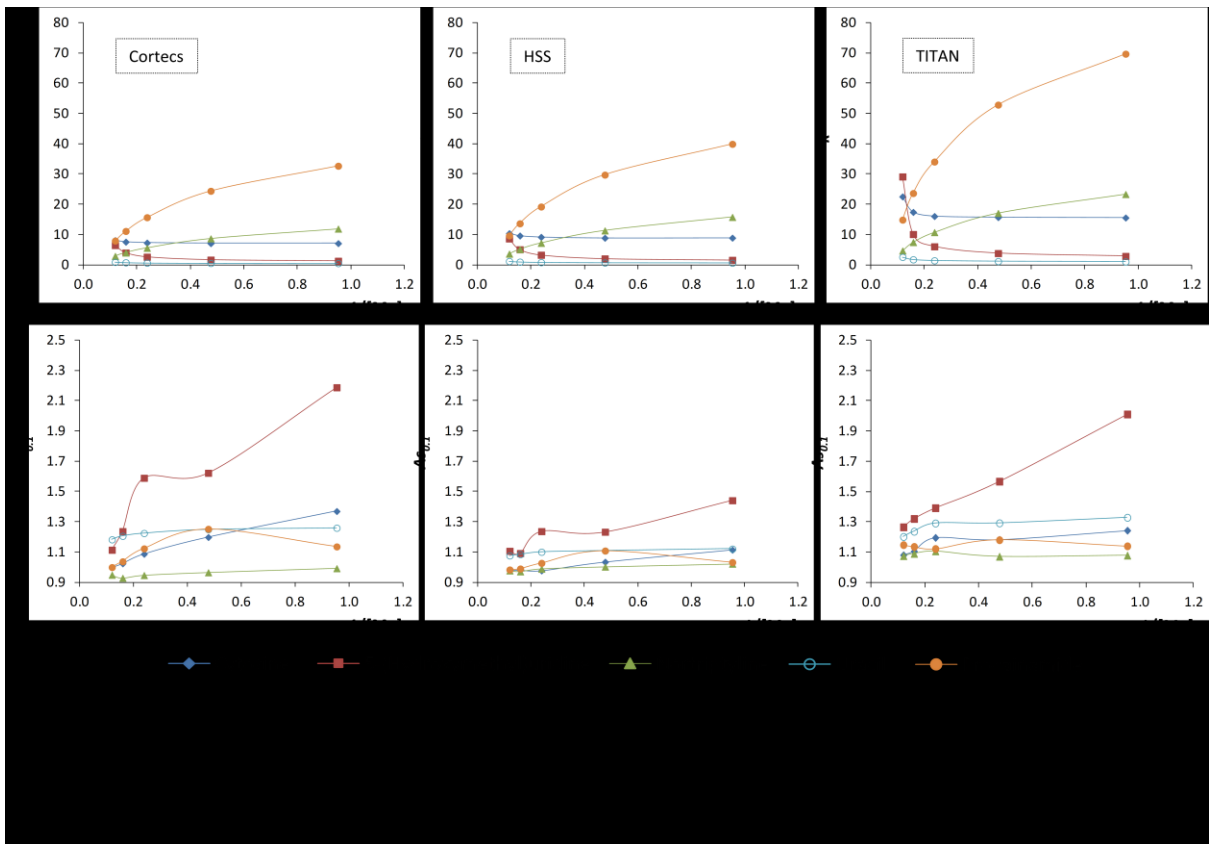
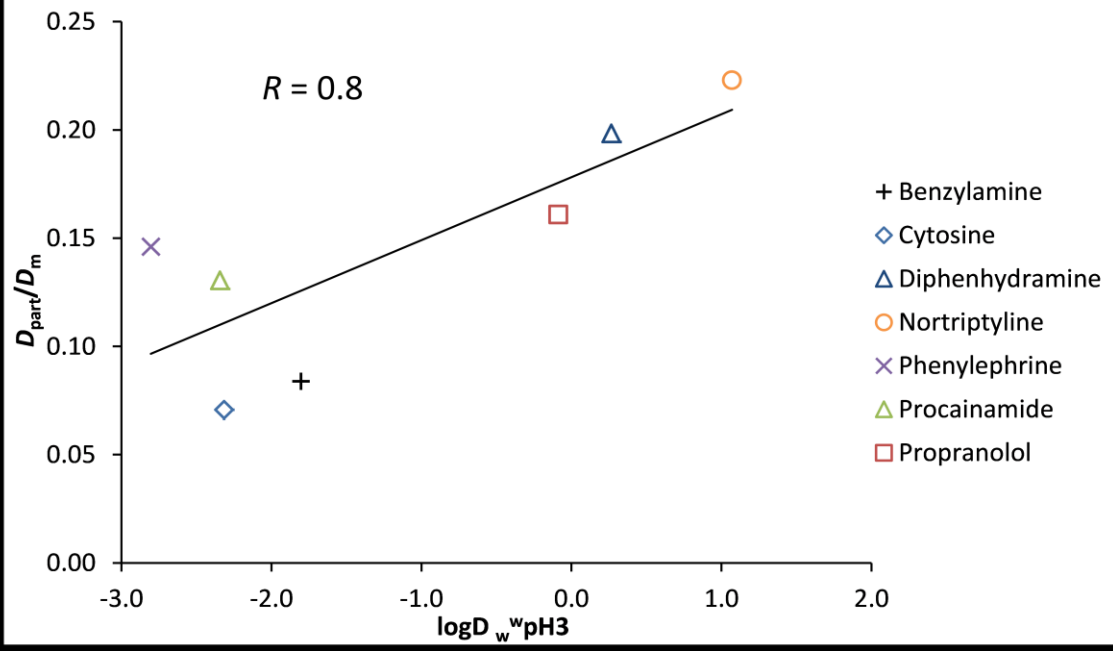












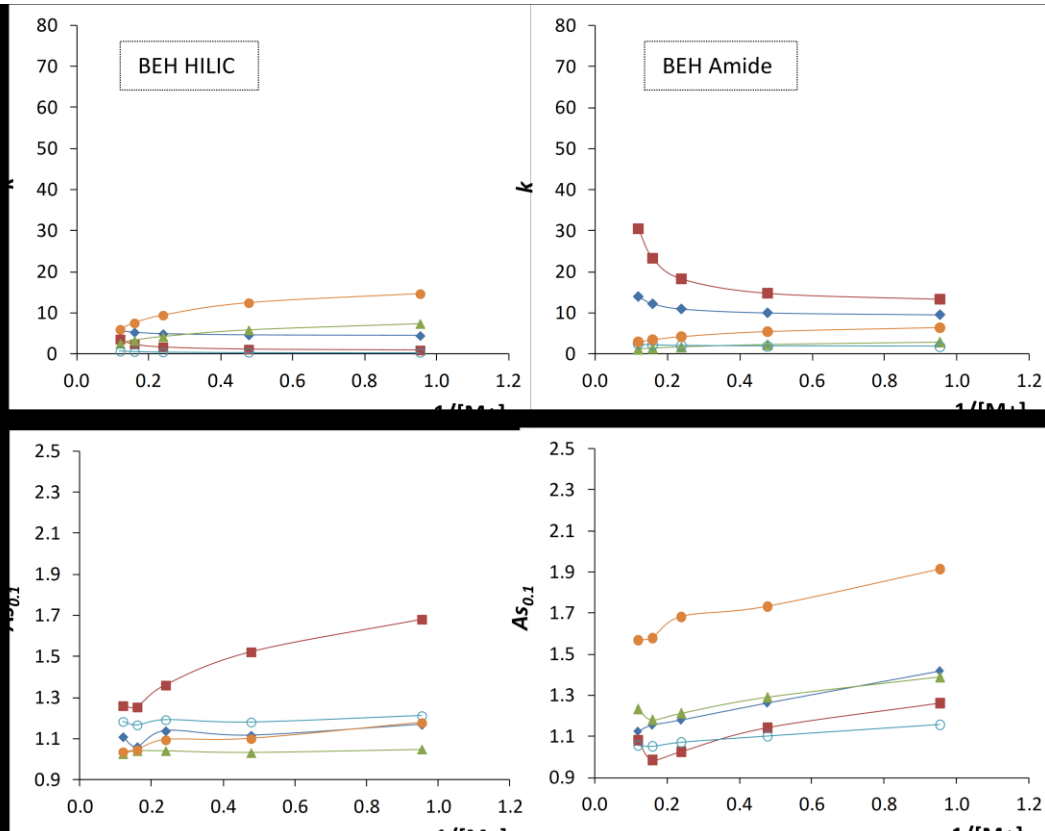


**Table 1. Preparation of mobile phases for van Deemter and arrested elution studies.**

Silica	Cytosine		Nortriptyline	
	% ACN	Buffer Concentration (mM/L)	% ACN	Buffer Concentration (mM/L)
Cortecs	93.7	5.2	94.8	4.2
BEH	94.8	5.2	94.8	2.6
HSS	93.2	5.2	94.8	5.2
TITAN	90.1	5.2	92.0	5.0

**Table 2. Manufacturers column characteristics and non-reduced van Deemter analysis using cytosine as a test solute.**

Silica	Particle size ( $\mu\text{m}$ )	$\rho$	Pore Size ( $\text{\AA}$ )	Surface Area ( $\text{m}^2/\text{g}$ )	$A$ ( $\times 10^{-4}$ cm)	$B$ ( $\times 10^{-5}$ $\text{cm}^2/\text{s}$ )	$C$ (ms)	$u_{\text{opt}}$ (cm/s)	$H_{\text{min}}$ ( $\times 10^{-4}$ cm)	$N_{\text{max}}$
Cortecs	1.6	0.7	90	100	1.3	3.8	0.32	0.35	3.5	28206
BEH	1.7	0	130	185	1.5	3.6	0.57	0.25	4.4	22720
HSS	1.8	0	100	230	2.0	3.8	0.57	0.26	4.9	20216
TITAN	1.9	0	80	410	2.2	3.2	0.57	0.24	4.8	20690

**Table 3. Flow resistance ( $\phi$ ) and permeability ( $K_{\text{vo}}$ ) measured for each column using cytosine elution conditions. Solvent viscosity was determined using reference [37].**

Silica	$\eta$ (cP)	$\phi$	$K_{\text{vo}}$ ( $\text{m}^2$ )
Cortecs	0.3861	462	5.55E-15
BEH	0.3777	432	6.69E-15
HSS	0.3899	413	7.85E-15
TITAN	0.4137	415	8.70E-15

**Table 4. Taylor-Aris derived solute diffusion coefficient ( $D_{\text{m}}$ ), effective diffusion ( $D_{\text{eff}}$ ) and reduced analysis from curve fitting and arrested elution experiments for different columns.**

Silica	$D_m$ (cm <sup>2</sup> /s)	$D_{eff}$ (cm <sup>2</sup> /s)	$D_{eff}/D_m$	$b$ (Peak Parking)	$b$ (Curve Fitting)	$C$ (Curve Fitting)	$v_{opt}$	$h_{min}$	$k'$ (Corrected)
Analyte = Cytosine									
Cortecs	1.84E-05	2.75E-06	0.15	2.04	2.04	0.23	3.00	2.22	5.8
BEH	1.88E-05	2.88E-06	0.15	2.00	1.90	0.37	2.26	2.59	5.5
HSS	1.79E-05	2.81E-06	0.16	2.28	2.10	0.23	3.01	2.36	6.2
TITAN	1.67E-05	2.85E-06	0.17	2.37	1.91	0.25	2.79	2.45	6.0
Analyte = Nortriptyline									
Cortecs	1.49E-05	3.64E-06	0.24	3.39	-	-	-	-	5.9
BEH	1.49E-05	4.21E-06	0.28	3.85	3.62	0.23	3.96	2.55	5.8
HSS	1.49E-05	3.84E-06	0.26	3.63	-	-	-	-	6.0
TITAN	1.40E-05	3.50E-06	0.25	3.52	-	-	-	-	6.0

**Table 5. Taylor-Aris derived solute diffusion coefficients ( $D_m$ ) and arrested elution data for different solutes on BEH HILIC silica including physiochemical parameters.**

Solute	% ACN	Buffer Concentration (mM/L)	$D_m$ (cm <sup>2</sup> /s)	$D_{eff}$ (cm <sup>2</sup> /s)	$D_{eff}/D_m$	$D_{part}/D_m$	$^1b$	$^2\log D_w^w$	pH3	MW (g/mol)	$k$ (Corrected)
Benzylamine	93.9	5.0	2.45E-05	4.03E-06	0.16	0.08	2.21	-1.80		107.2	5.7
Cytosine	94.8	5.2	1.88E-05	2.88E-06	0.15	0.07	2.00	-2.32		111.1	5.5
Diphenhydramine	95.0	2.9	1.62E-05	4.34E-06	0.27	0.20	3.53	0.27		255.4	5.6
Nortriptyline	94.8	2.6	1.49E-05	4.21E-06	0.28	0.22	3.85	1.07		263.4	5.8
Phenylephrine	93.4	5.0	1.42E-05	3.18E-06	0.22	0.15	2.99	-2.80		167.2	5.7
Procainamide	92.3	5.0	1.43E-05	2.97E-06	0.21	0.13	2.84	-2.34		235.3	5.8
Propranolol	95.0	2.3	1.46E-05	3.45E-06	0.24	0.16	3.14	-0.09		259.3	5.6

<sup>1</sup>Calculated using Eqn. 7

<sup>2</sup>logD values were averaged from ACD/ Marvin/ MedChem Designer